Supporting Information for:

Triazatriangulene as Binding Group for Molecular Electronics

Zhongming Wei,[†,§,‡] Xintai Wang,[†,‡] Anders Borges,[†] Marco Santella,[†,§] Tao Li,[†] Jakob Kryger Sørensen,[†] Marco Vanin,[†] Wenping Hu,[⊥] Yunqi Liu,[⊥] Jens Ulstrup,[#] Gemma C. Solomon,[†] Qijin Chi,[#] Thomas Bjørnholm,[†] Kasper Nørgaard,[†,*] and Bo W. Laursen[†,*]

[†]Nano-Science Center & Department of Chemistry, University of Copenhagen, Universitetsparken 5, DK-2100 Copenhagen Ø, Denmark

[§]Sino-Danish Centre for Education and Research (SDC), Niels Jensens Vej 2, DK-8000 Aarhus C, Denmark

[⊥]Beijing National Laboratory for Molecular Sciences, Key Laboratory of Organic Solids, Institute of Chemistry, Chinese Academy of Sciences, Beijing 100190, China

[#]Department of Chemistry and NanoDTU, Technical University of Denmark, Building 207, Kemitorvet, 2800 Lyngby, Denmark

Corresponding Author

*kn@nano.ku.dk; bwl@nano.ku.dk

Author Contributions

‡These authors contributed equally.

Contents:

1. Synthesis part.

General Methods

Chemicals were bought from Aldrich and used as received. 4,8,12-Tri-*n*-octyl-4,8,12-triazatriangulenium tetrafluoroborate (TATA$^+$BF$_4^-$) was synthetized according to a literature procedure.[1] Thin layer chromatography was carried out using aluminum sheets precoated with silica gel 60F (Merck 5554). Flash column chromatography was carried out using ROCC silica gel (0.040-0.063 mm). All reactions were performed under inert atmosphere using solvents that had been carefully flushed (degassed) with inert atmosphere before use. THF was distilled over Na / benzophenone. ^{1}H- and ^{13}C-NMR spectra were recorded on a Bruker instrument using residual solvent signals for calibration (500/125 MHz). All coupling constant are expressed in Hertz (Hz). Mass spectrometry (MS) was performed using Matrix Assisted Laser Desorption Ionization (MALDI); HR = High Resolution. Elemental analysis was performed at Copenhagen University.

**4,8,12-Tri-*n*-octyl-4,8,12-triazatriangulenium tetraphenylborate (TATA-Ph$_4$B)**
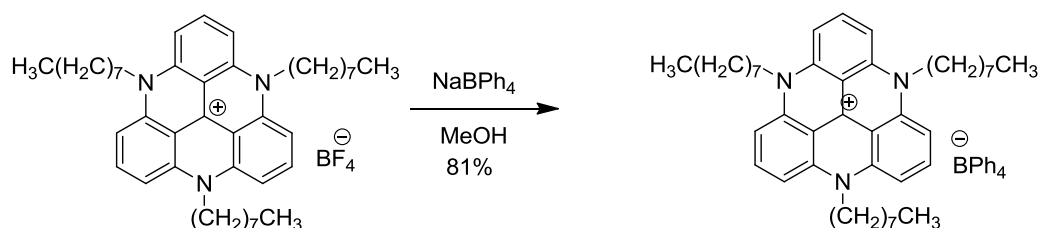
TATA$^+$ BF$_4^-$ (1 g, 1,4 mmol) was dissolved in boiling MeOH (350 mL) and NaBPh$_4$ (1 g, 2.9 mmol) dissolved in a minimum amount of MeOH (ca. 2 mL) added to the resulting solution. A thick, brightly red precipitate formed immediately. The suspension was left overnight at -18 ºC and the product was filtered off and washed with cold MeOH and H$_2$O to give the product as red crystals. Yield 1,1 g, 81%. ^{1}H NMR (500 MHz, DMSO-d6) δ 7.99 (t, *J* = 8.3 Hz, 3H), 7.26 (d, *J* = 8.3 Hz, 6H), 7.20 – 7.14 (m, 8H), 6.91 (t, *J* = 7.3 Hz, 8H), 6.78 (t, *J* = 7.3 Hz, 4H), 4.24 – 4.21 (m, 6H), 1.73 – 1.70 (m, 6H), 1.56 – 1.60 (m, 6H), 1.42 – 1.34 (m, 6H), 1.34 – 1.25 (m, 18H), 0.90 – 0.83 (m, 9H) ppm. ^{13}C NMR (125 MHz, DMSO) δ 163.33 (q, J_{C-B} = 49.4 Hz), 139.69, 139.49, 137.65, 135.51 (q, J_{C-B} = 1.4 Hz), 125.26 (q, J_{C-B} = 2.7 Hz), 121.47, 109.72, 105.00, 46.96, 31.22, 28.79, 28.73, 25.91, 24.55, 22.08, 13.96. MALDI-TOF (dithranol matrix) m/z 618.57 (M$^+$). Anal. Found C: 85.60; H: 8.46; N: 4.46 Calcd. For C$_{67}$H$_{80}$BN$_3$, C: 85.77 ; H: 8.59; N: 4.48.

^{1}H NMR for TATA tetraphenylborate:

## ^{13}C NMR for TATA tetraphenylborate:

S3

TATA 1 (12c-Phenyl-4,8,12-tri-n-octyl-4,8,12-triazatriangulene)

TATA **1** was also reported previously by **R. Herges** *et al.*.[2,3]
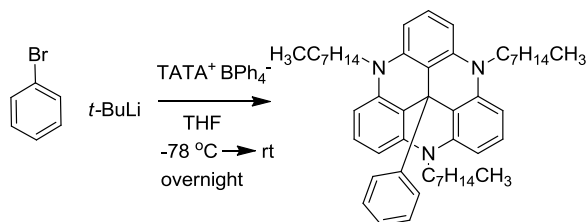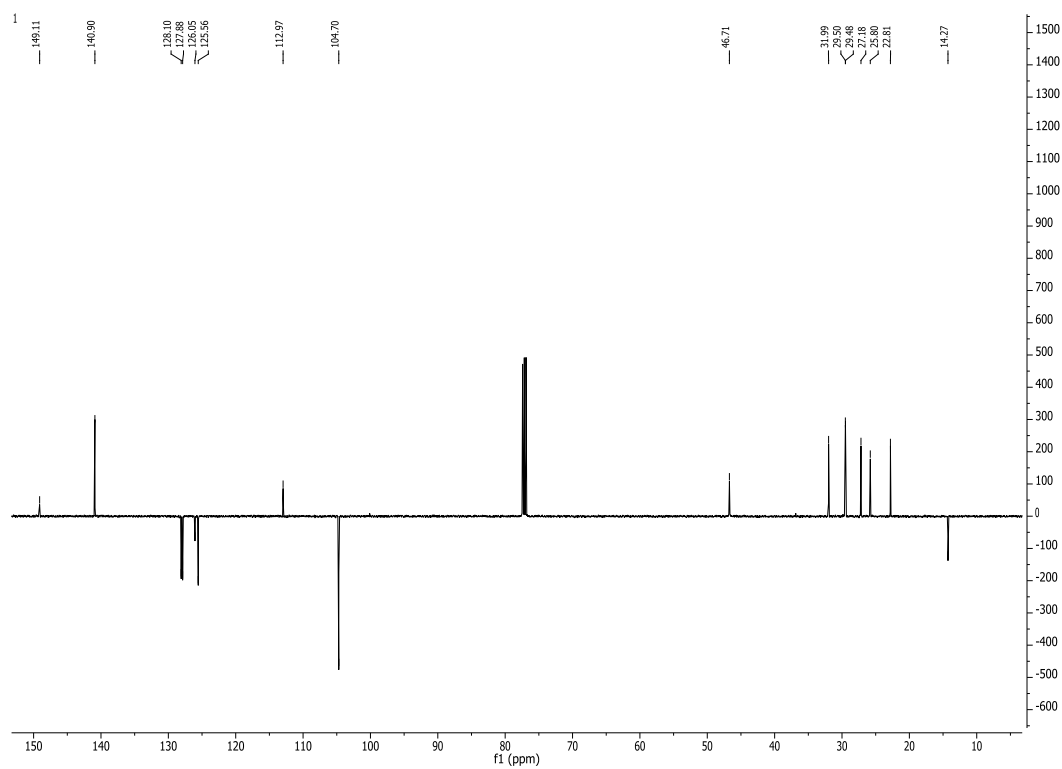

Bromobenzene (65 mg, 0.42 mmol) was dissolved in dry freshly distilled THF (5 mL) under argon and cooled to -78°C. *t*-butyl lithium (0.50 mL, 1.7 M in hexane, 0.86 mmol) was then added drop-wise. The components were allowed to react at -78 °C for 60 minutes. Triangulenium BPh_4 salt (130 mg, 0.21 mmol) was then added all at once as solid. The reaction was left to stir under argon overnight covering the reaction vessel with aluminium foil in order to avoid decomposition of the target material on exposure to light. The solution was then diluted (Et_2O, 100 mL) and filtered through a short Al_2O_3 plug (Et_2O as eluent). The residue was purified by column chromatography (Al_2O_3, 5:1 heptane : Et_2O,) to furnish the product **1** as a white solid (85 mg, 57%). ^{1}H NMR (500 MHz, $CDCl_3$) δ 7.17 (t, *J* = 8.3 Hz, 3H), 7.01 – 6.90 (m, 3H), 6.87 – 6.83 (m, 2H), 6.53 (d, *J* = 8.3 Hz, 6H), 3.88 – 3.78 (m, 6H), 1.85 – 1.74 (m, 6H), 1.41 – 1.25 (m, 30H), 0.94 – 0.85 (m, 9H). ^{13}C NMR (125 MHz, $CDCl_3$) δ 149.11, 140.90, 128.10, 127.88, 126.05, 125.56, 112.97, 104.70, 46.71, 31.99, 29.50, 29.48, 27.18, 25.80, 22.81, 14.27. one signal missing. MALDI+ *m/z*: 697.35 [MH]$^+$; calcd for $C_{49}H_{66}N_3^+$: 696.52
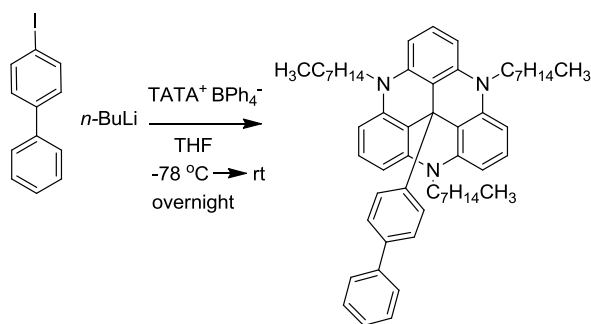
^{1}H NMR for **TATA 1**:
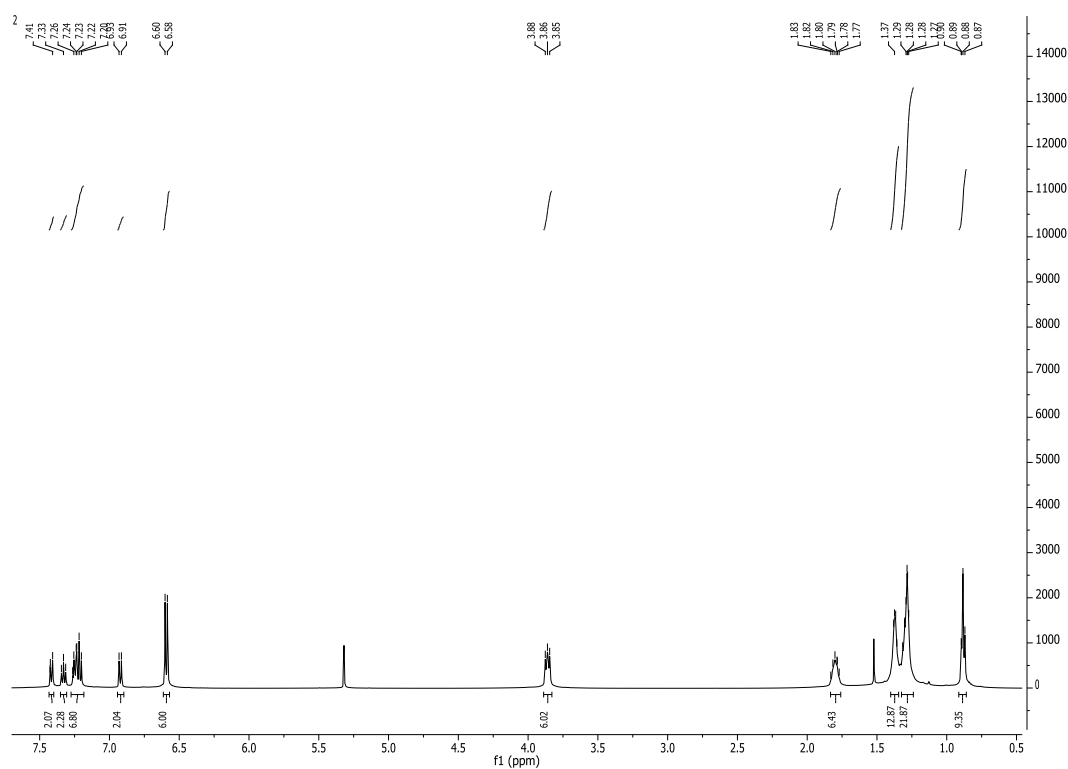

^{13}C NMR for **TATA 1**:

S5
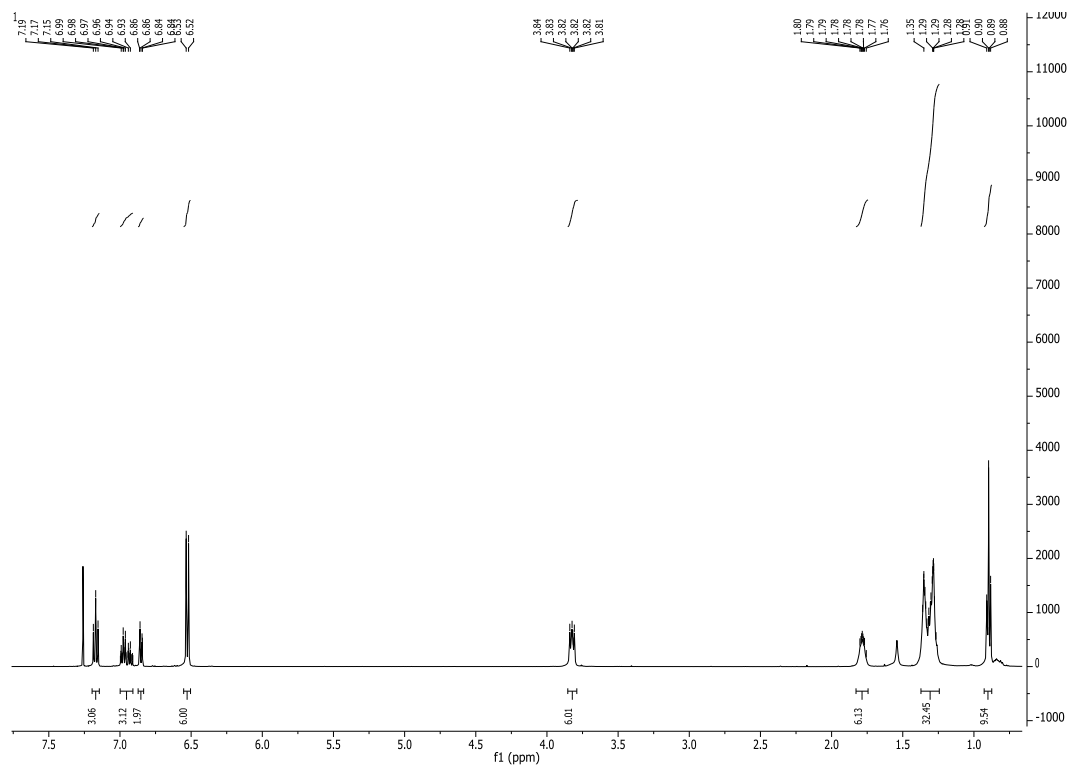
TATA 2 (12*c*-4,4'-Biphenyl-Phenyl-4,8,12-tri-*n*-octyl-4,8,12-triazatriangulene)
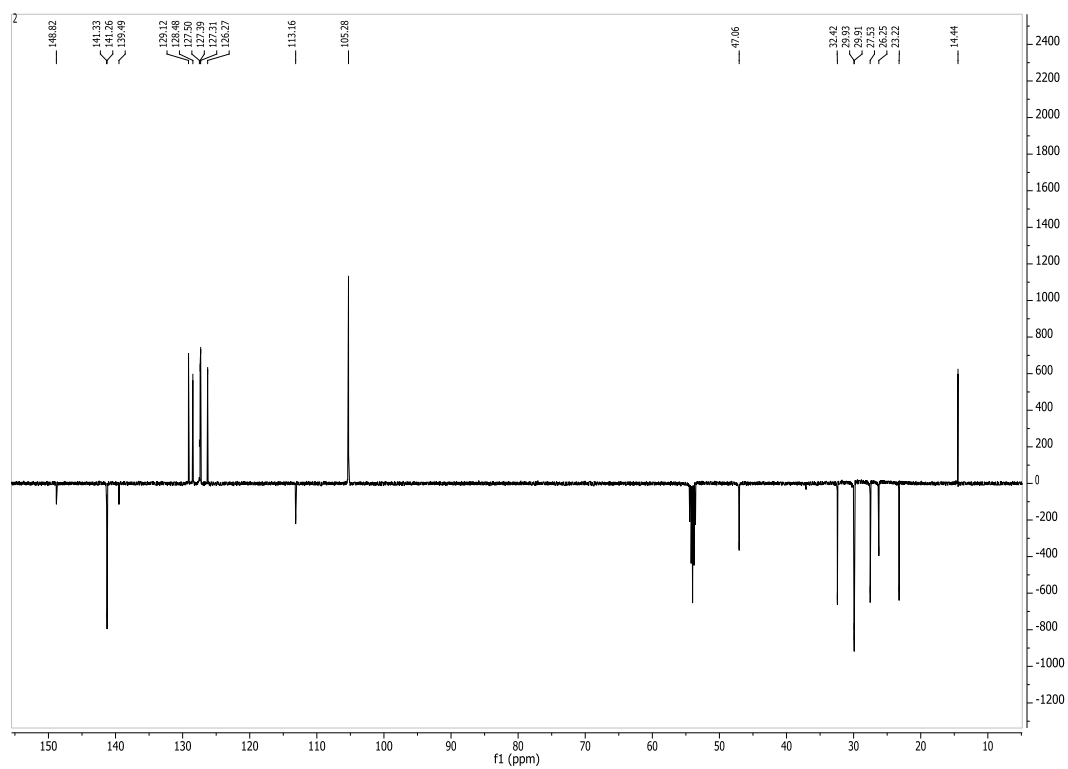

4-iododiphenyl (300 mg, 1.1 mmol) was dissolved in dry freshly distilled THF (20 mL) under argon and cooled to -78ºC. *n*-butyl lithium (0.52 mL, 2.5 M in hexane, 1.3 mmol) was then added drop-wise. The components were allowed to react at -78 ºC for 60 minutes. Triangulenium BPh_4 salt (250 mg, 0.27 mmol) was dissolved in 20 mL THF degassed by dry argon and the previously generated lithium species added to the resulting red solution via canula. The reaction was left to stir under argon overnight with the reaction vessel covered with aluminium foil to avoid decomposition of the target material on exposure to light. The solution was then diluted (Et_2O, 100 mL) and filtered through a short silica plug (Et_2O as eluent). The residue was purified by column chromatography (SiO_2, 5:1 heptane : CH_2Cl_2,) to furnish the product **2** as a white solid (44 mg, 21%). ^{1}H NMR (500 MHz, CD_2Cl_2) δ 7.43 – 7.40 (m, 2H), 7.33 (t, *J* = 7.6 Hz, 2H), 7.28 – 7.18 (m, 6H), 6.92 (d, *J* = 8.5 Hz, 2H), 6.59 (d, *J* = 8.3 Hz, 6H), 3.89 – 3.83 (m, 6H), 1.83 – 1.77 (m, 6H), 1.38 – 1.36 (m, 12H), 1.32 – 1.27(m, 18H), 0.90 – 0.87 (m, 9H). ^{13}C NMR (125 MHz, CD_2Cl_2) δ 148.82, 141.33, 141.26, 139.49, 129.12, 128.48, 127.50, 127.39, 127.31, 126.27, 113.16, 105.28, 47.06, 32.42, 29.93, 29.91, 27.53, 26.25, 23.22, 14.44 one signal missing. HR-MS (MALDI+) *m/z*: 772.5570 [MH]$^+$; calcd for $C_{55}H_{70}N_3^+$: 772.5570
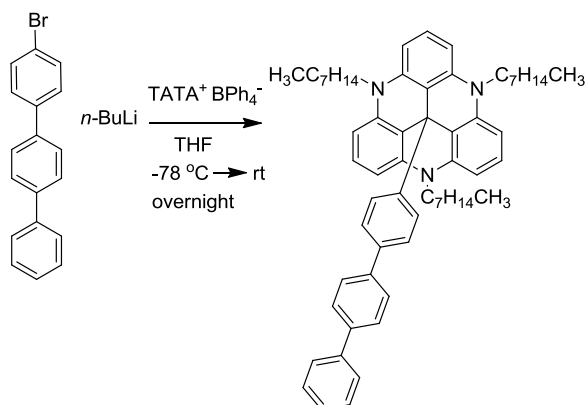
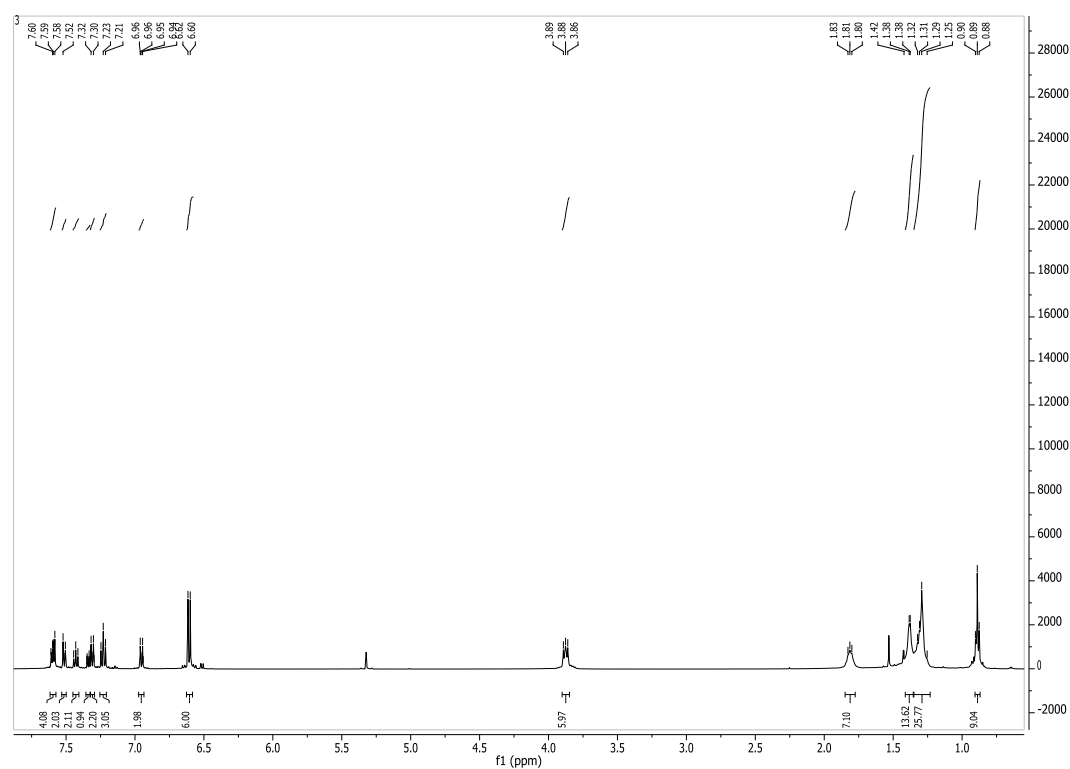# ¹H NMR for **TATA 2**:

¹³C NMR for **TATA 2**:

## TATA 3 (12c-1,1',4',1''-Terphenyl-4,8,12-tri-n-octyl-4,8,12-triazatriangulene)

4-bromo-p-terphenyl (300 mg, 0.97 mmol) was dissolved in dry freshly distilled THF (20 mL) under argon, cooled to -78ºC, and n-butyl lithium (0.47mL, 2.5 M in hexane, 1.2 mmol) added drop-wise. The components were allowed to react at -78 ºC for 60 minutes. Triangulenium BPh_4 salt (230 mg, 0.25 mmol) was dissolved in 20 mL THF degassed in dry argon and the previously generated lithium species added to the resulting red solution via canula. The reaction was left to stir under argon overnight covering the reaction vessel with aluminium foil in order to avoid decomposition of the target material on exposure to light. The solution was then diluted (Et_2O, 100 mL) and filtered through a short silica plug (Et_2O as eluent). The residue was purified by column chromatography (SiO_2, 7:1 heptane : CH_2Cl_2,) to furnish the product **3** as a white solid (67 mg, 32%). ^{1}H NMR (500 MHz, CD_2Cl_2) δ 7.62 – 7.57 (m, 4H), 7.53 – 7.50 (m, 2H), 7.43 (t, J = 7.7 Hz, 2H), 7.35 – 7.29 (m, 1H), 7.32 – 7.29 (m, 2H), 7.23 (t, J = 8.3 Hz, 3H), 6.97 – 6.93 (m, 2H), 6.61 (d, J = 8.3 Hz, 6H), 3.90 – 3.85 (m, 6H), 1.85 – 1.78 (m, 6H), 1.41 – 1.35 (m, 12H), 1.32 – 1.25 (m, 18H), 0.91 – 0.87 (m, 9H). ^{13}C NMR (125 MHz, CD_2Cl_2) δ 148.95, 141.28, 141.17, 141.10, 140.25, 138.91, 129.32, 128.50, 127.80, 127.74, 127.41, 127.20, 126.35, 113.17, 112.69, 105.30, 104.79, 47.06, 32.44, 29.95, 29.93, 27.55, 26.27, 23.23, 14.46. HR-MS (MALDI+) m/z: 848.5894 [MH]$^+$; calcd for $C_{61}H_{74}N_3^+$: 848.5883

^{1}H NMR for **TATA 3**:

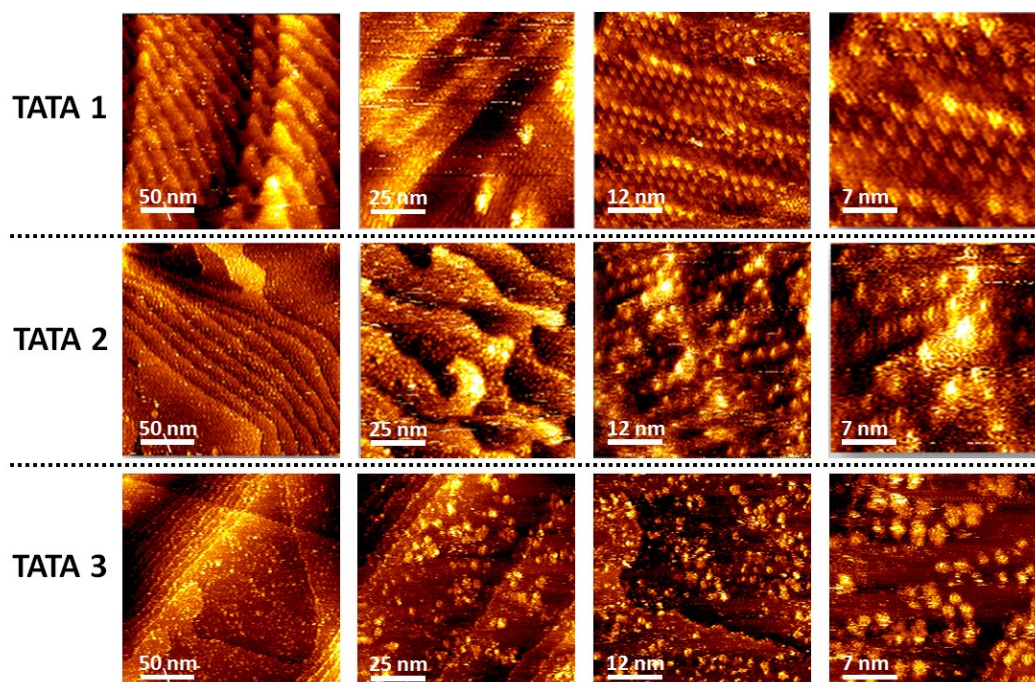

^{13}C NMR for **TATA 3**:
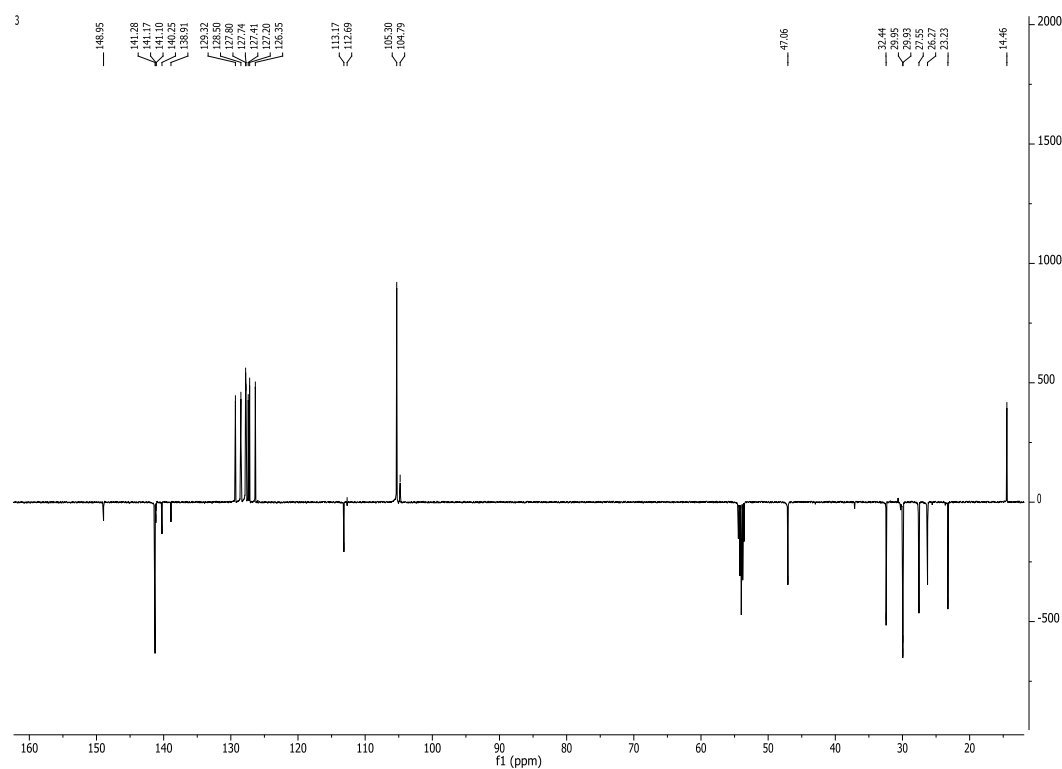
2. EC-STM of TATA **1-3** SAMs.

Figure S1. EC-STM images for TATA **1**, **2** and **3** (from top to bottom). Scan area = 200×200 nm^2, 100×100 nm^2, 50×50 nm^2, 30×30 nm^2. Solution pH = 1.69, working potential = -0.1 V vs. SCE, bias voltage = -1.2 V~-0.9 V, tunneling current setpoint = 30 pA ~ 35 pA.

Table S1. Summary the EC-STM results of TATA **1-3** SAMs.

Molecule	TATA 1	TATA 2	TATA 3
Small Terrace	Covered	Covered	Covered
Large Terrace	Covered	Uncovered	Covered
Shape	Triangular	Triangular like with white spots	Triangular like with white spots
Center to center distance	1.4 nm	1.4 nm	2.1 nm
Mean molecular area (footprint)	1.7 nm^2	1.7 nm^2	3.8 nm^2
Surface packing	Hexagonal	Random	Random

3. Cyclic voltammetry and water contact angles of the SAMs.

Figure S2 shows cyclic voltammograms of an aqueous 10 mM K$_3$[Fe(CN)$_6$]/K$_4$[Fe(CN)$_6$] solution, recorded with the SAMs on Au as electrode. Compared to the bare Au electrode, the peaks for the Fe(II)/Fe(III) redox signal totally disappear when the SS1-3 and S3 SAMs cover the Au surface (Figure S2), showing that these SAMs form high-density SAMs that block the Fe(II)/Fe(III) redox process completely. Unfortunately, we could not get high quality SAM for S1 and S2. Although their CV showed clear Fe(II)/Fe(III) redox signal, these signals had decreased and were shifted towards negative potentials with significantly increased peak separation (Figure S2b). This implies that the S1 and S2 SAMs block access to the Au surface partly, but the SAM densities were not as high as for SS1-3.
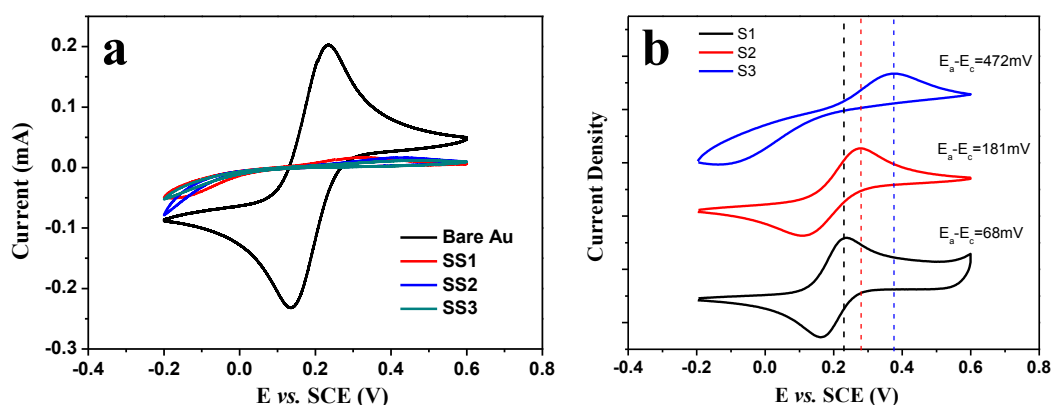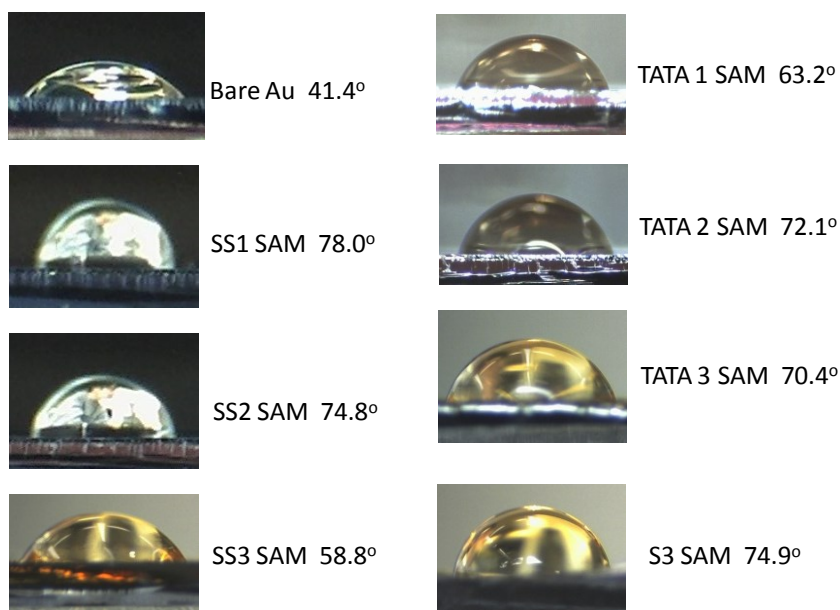

Figure S2. Cyclic voltammograms of (a) bare Au and SS1-3 SAMs on Au; (b) S1-3 SAMs on Au.
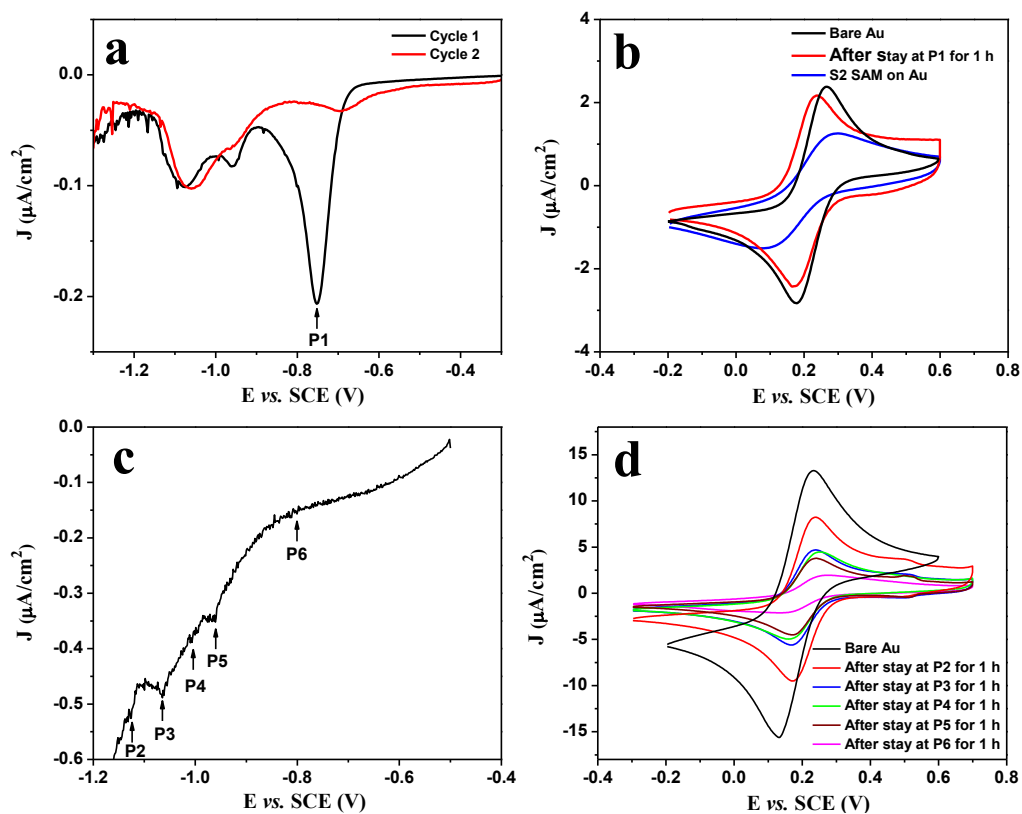
Figure S3. Enlarged reductive linear sweep desorption voltammograms and corresponding cyclic voltammograms (in $K_3[Fe(CN)_6]/K_4[Fe(CN)_6]$ solution) for S2 (a, b) and TATA **2** (c, d) SAMs. For S2 almost all molecules was desorbed from the surface after 1 h at $E_D = -0.75$ V vs. SCE as shown by the desorption peak at P1, Figure 3a. For TATA **2**, no obvious desorption peak appeared and several different potential values (P2-P6, Figure S3c) were used to check the stability.

Water contact angles on the SAMs were determined by depositing a drop (~1 µL) of pure water (MILLI-Q, 18 MΩ•cm) on the SAM surface. The contact angles were determined from optical images a few seconds after application of the drop and captured by a home-made camera. Figure S4 shows the water contact angles of bare Au and the SAMs. All the SAMs had much higher contact angles than bare Au which means that these molecules made the Au surface more hydrophobic.

Bare Au 41.4°

TATA 1 SAM 63.2°

SS1 SAM 78.0°

TATA 2 SAM 72.1°

SS2 SAM 74.8°
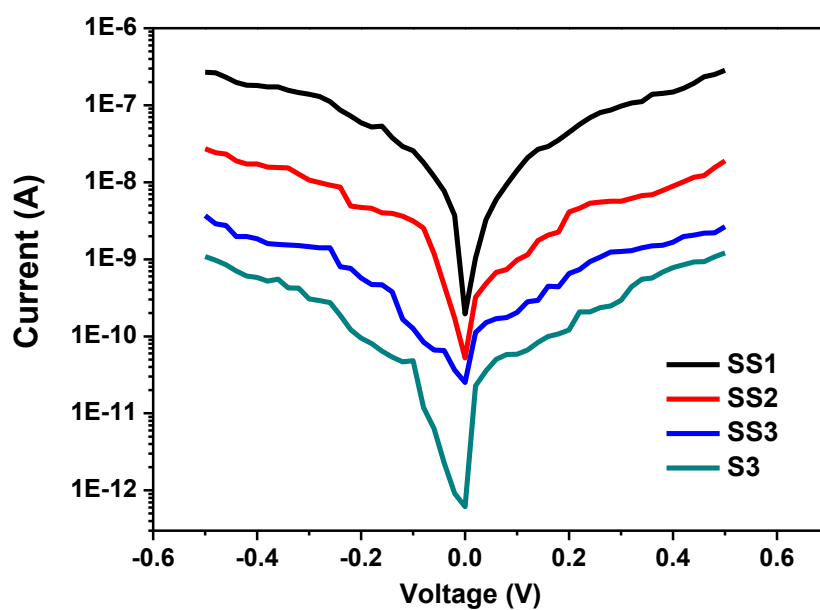
TATA 3 SAM 70.4°

SS3 SAM 58.8°

S3 SAM 74.9°

Figure S4. Water contact angles of bare Au and the SAMs.

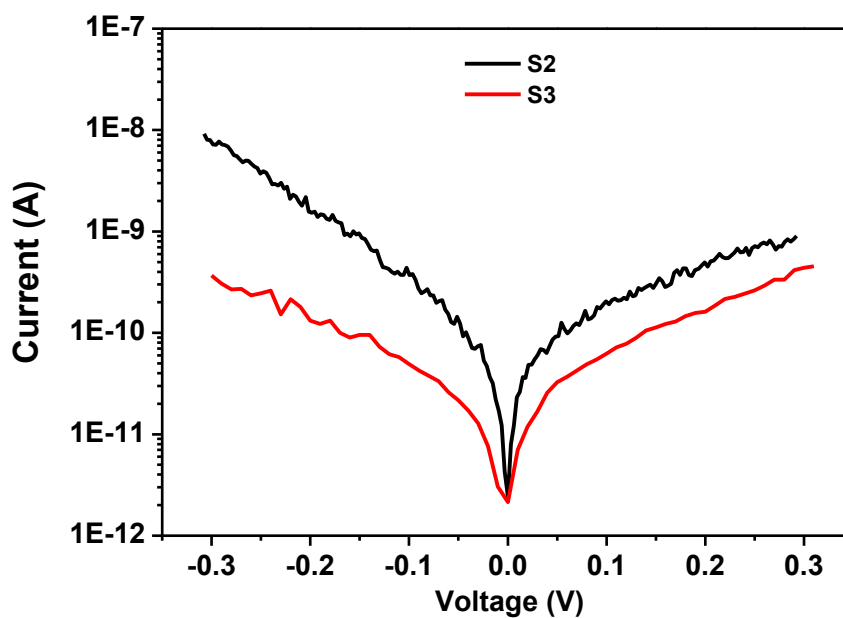**4.** UV-Vis absorption spectra for the TATA **1-3**.
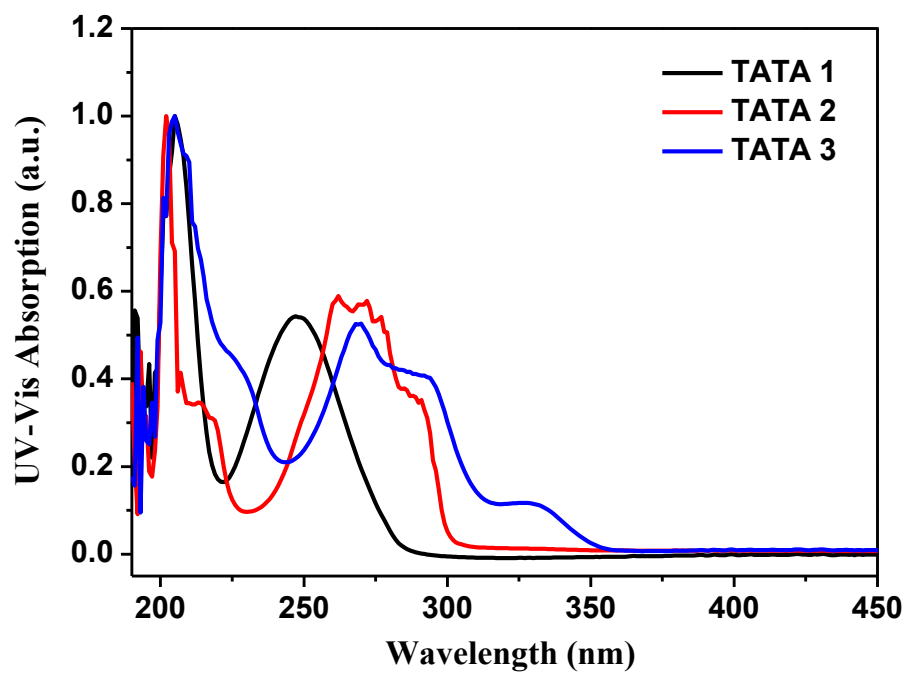
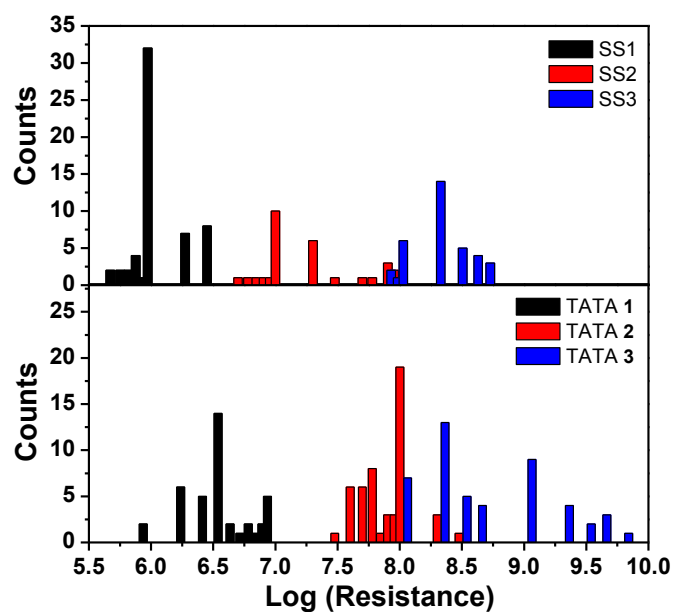**Figure S5.** UV-Vis absorption spectra of TATA **1-3** in ethanol solutions.

5. More CP-AFM and EC-STM *I-V* curves and resistance histograms of the molecular junctions.

Figure S6. Typical *I-V* curves of the molecular junctions based on SS1-3 and S3 SAMs recorded by CP-AFM.

Figure S7. Typical *I-V* curves of the molecular junctions based on S2 and S3 SAMs recorded by EC-STM.

Figure S8. Resistance histograms of SS1-3 and TATA **1**-**3** molecular junctions recorded by CP-AFM.
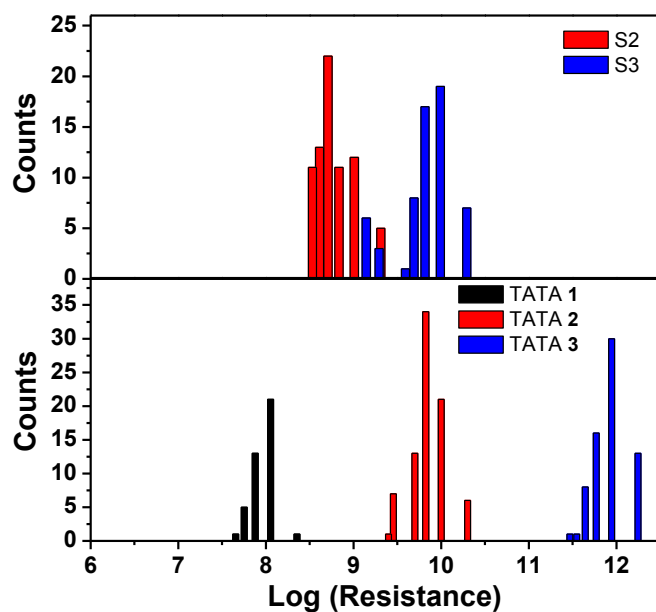
Figure S9. Resistance histograms of the EC-STM recorded for S2-3 and TATA **1**-**3** molecular junctions.

6. Calculated junction structures for all molecules, local currents throughout the

bandgap for TATA, transmission, and PDOS for SS1-3

**Computational details**: All structures were optimized using the ASE/GPAW packages.

Gas-phase structures:

The gas-phase molecules were structurally optimized using the finite difference mode with a grid spacing of 0.18 Å. A vacuum of at least 3.0 Å was used and exchange and correlation was included with the PBE functional. The structures were relaxed until the maximum force on any atom was below 0.01 eV/Å.

Surface structures:

The geometry of the bare TATA platform optimized in vacuum was placed on a 6x6x3 Au fcc(111) surface with a vacuum of 13 Å in the direction normal to the surface. The positions of the Au atoms were kept fixed while the TATA structure was relaxed until the maximum force on any atom was below 0.05 eV/Å. A double zeta basis set with polarization functions was used. The density was represented on a grid with a spacing of 0.18 Å and the Langreth-Lundqvist vdW-DF2 functional with the Cooper exchange C09 functional used. Periodic boundary conditions were employed and a Monckhorst-Pack k-point sampling of (2,2,1) was used.

The gas-phase optimized and surface optimized structure of the bare TATA-platform using identical settings are shown below. A slight flattening of the molecule is observed on the surface. The gas-phase optimized molecular wires were attached to the bare TATA-platform without further relaxation using binding lengths from the gas-phase geometry.
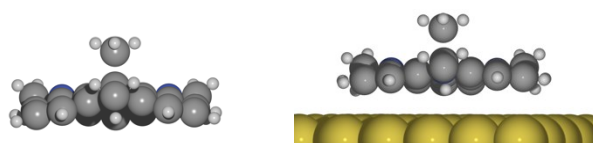
Figure S10. Gas-phase optimized TATA (left) and surface optimized TATA (right).

The gas-phase optimized thiols were chemisorbed (H's removed) onto an fcc(111) hollow site with a vertical distance to the Au surface of 2.04 Å. This distance is based on a Morse potential fitted to an adsorbtion curve using the PBE functional. The distance from the terminal hydrogen to the other electrode was set to 2.4 Å for both TATA and thiol-based junctions. No binding was observed using the PBE functional so the distance of 2.4 was chosen to mimic weak contact based on an adsorbtion curve. Different binding distances were tested and found to yield similar results.

The geometries of the scattering regions used for the transport calculations with the ASE transport module are shown below:
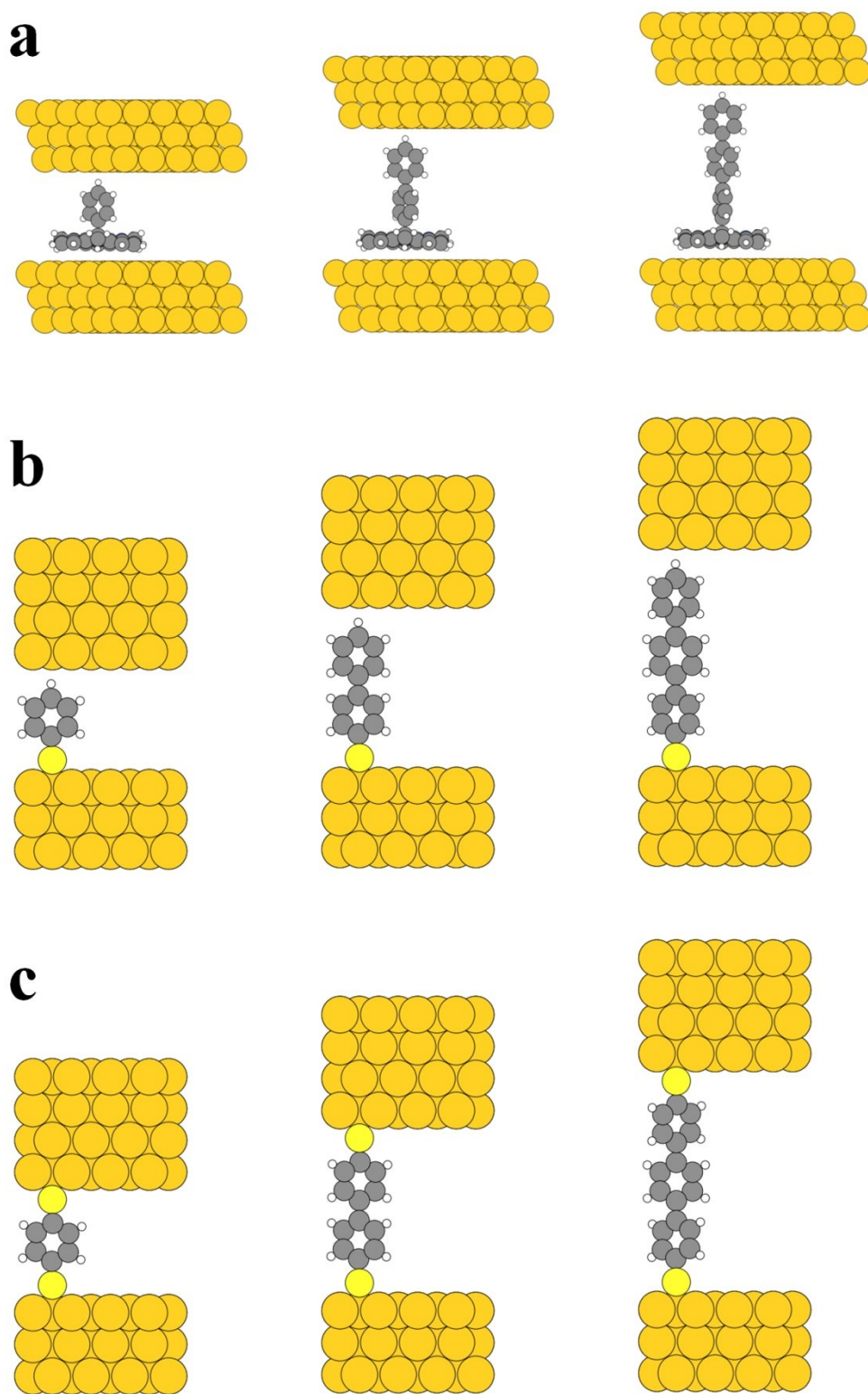
Figure S11. Junction geometries used for DFT transport calculations: (a) TATA **1-3**; (b) S1-3; (c) SS1-3.

Local currents:

Figure S12 shows the local currents throughout the band-gap. It is clear that no single path dominates charge injection into the TATA **1**.
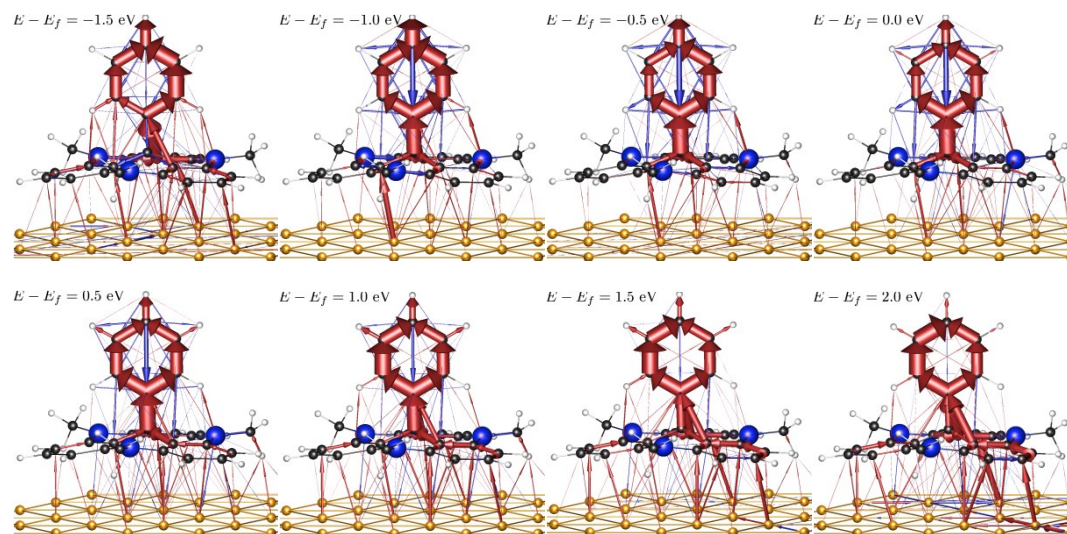

Figure S12. Local currents calculated for TATA **1**. An arrow is drawn between to atoms if the contribution to the total transmission exceeds 0.5 % of the total transmission. Blue (red) arrows indicate positive (negative) contributions.

Transmission and PDOD for SS1-3:

Zero-bias transmissions were calculated using LCAO mode with standard GPAW settings and Monckhorst-Pack k-point sampling of 3x3x1 for the TATAs and 4x4x1 for the thiols. Projected density of states (PDOS) were calculated from the Green's function for each element in the local basis set centered on atoms on the molecule. Contributions from atoms belonging to the anchoring group (S atoms or TATA platform) or wire (remaining molecular atoms) were summed to produce the projected density of states.

The transmission and PDOS for the SS(1-3) molecules calculated by ASE are shown in Figure S13.
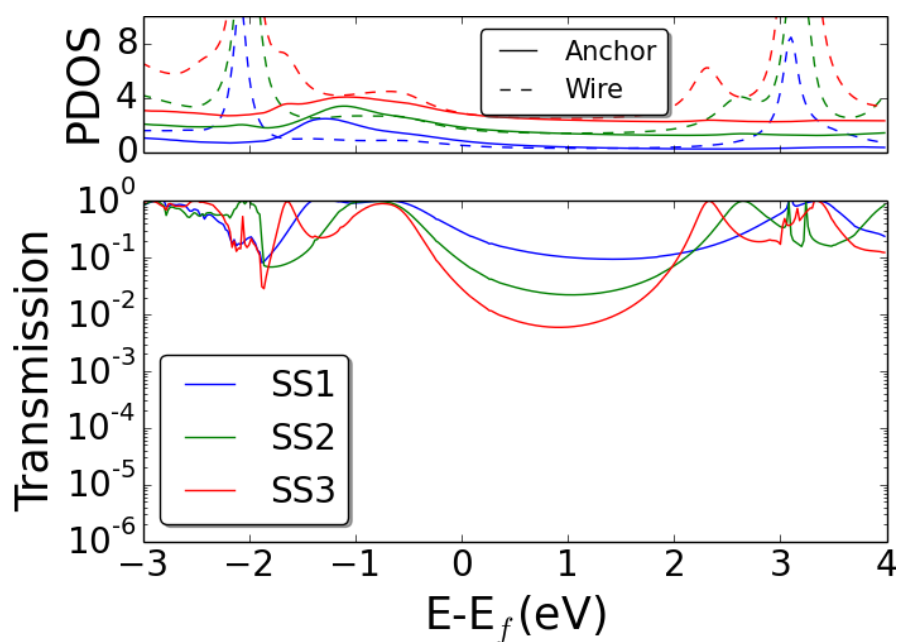
Figure S13. Transmission and PDOS for SS1-3.

gDFTB calculations:

The junctions used for the gDFTB calculations all used 6×6×3 leads on both sides. The vertical distance from the plane of the Au to the H/S was changed to 1.8 Å/2.8. Otherwise the structures were identical to those described above. Figure S14 shows the transmission calculated using gDFTB. The Fermi energy was taken to be -5 eV. The peaks in the TATA transmissions at $E-E_f \sim$-0.5 eV correspond to the TATA peak from the DFT calculations. This peak was only clear for the shortest wire in the DFT calculations. Still, the gDFTB calculations agree qualitatively with the DFT calculations and justify the use of the local current description.
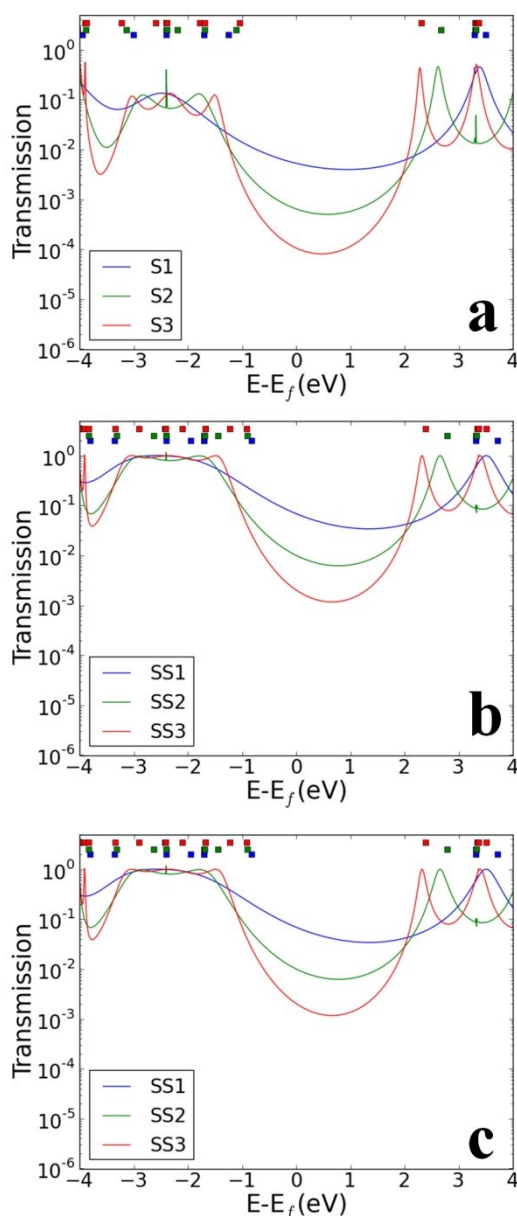
Figure S14. Calculated transmission for (a) S1-3 and (b) SS1-3 and (c) TATA **1-3**. Squares above the graph indicate the eigenvalues of the subset of the junction Hamiltonian corresponding to the molecule.

References:

1. Laursen, B. W.; Krebs, F. C. *Chem. Eur. J.* **2001**, *7*, 1773-1783.

2. Baisch, B.; Raffa, D.; Jung, U.; Magnussen, O. M.; Nicolas, C.; Lacour, J.; Kubitschke, J.; Herges, R. *J. Am. Chem. Soc.* **2009**, *131*, 442-443.

3. Kubitschke, J.; Näther, C.; Herges, R. *Eur. J. Org. Chem.* **2010**, 5041-5055.